# TITLE:
# A Field Study to Assess the Role of Air-Water Interfacial Sorption on PFAS Leaching in an AFFF Source Area

AUTHORS: Charles E. Schaefer[1,*], Graig M. Lavorgna[2], David R. Lippincott[2], Dung Nguyen[3], Emerson Christie[4], Stefanie Shea[5], Sean O'Hare[1], Maria C.S. Lemes[3], Christopher P. Higgins[5], Jennifer Field[4]

AFFILIATIONS:

[1] CDM Smith, 110 Fieldcrest Avenue, #8, 6th Floor, Edison, NJ 08837

[2] APTIM Federal Services, 17 Princess Rd, Lawrenceville, NJ 08648

[3] CDM Smith, 14432 SE Eastgate Way, # 100, Bellevue, WA 98007

[4] 1007 Agricultural and Life Science Building, Department of Molecular and Environmental Toxicology, Oregon State University, Corvallis, OR 97331

[5] Department of Civil and Environmental Engineering, Colorado School of Mines, Golden, CO 80401

[*]**CORRESPONDING AUTHOR**: Mailing address: CDM Smith, 110 Fieldcrest Avenue, #8, 6th Floor, Edison, NJ 088837. (732)-590-4633. E-mail: schaeferce@cdmsmith.com

**Abstract**

Field-deployed lysimeters were used to measure the concentrations of poly- and perfluoroalkyl substances (PFASs) in soil porewater at a site historically impacted with aqueous film forming foam (AFFF). Samples collected over a 49-day period showed that perfluorooctane sulfonate (PFOS) and perfluorohexane sulfonate (PFHxS) were the PFASs with the highest concentrations in porewater, with concentrations of approximately 10,000 and 25,000 ng $L^{-1}$, respectively. The corresponding average mass flux to underlying groundwater observed for PFOS and PFHxS was 28,000 ± 11,000 and 92,000 ± 32,000 ng $m^{-2}$ $d^{-1}$, respectively. Employing the use of batch desorption isotherms (soil:water slurries) to determine desorption $K_d$ values resulted in an overestimation of PFAS porewater concentrations by a factor for 1.4 to 4. However, using the desorption $K_d$ values from the batch desorption isotherms in combination with a PFAS mass balance that incorporated PFAS sorption at the air-water interface resulted in improved predictions of the PFAS porewater concentrations. This improvement was most notable for PFOS, where inclusion of air-water interfacial sorption resulted in a 58% reduction in the predicted PFOS porewater concentration and predicted PFOS porewater concentrations that were identical (within the 95% confidence interval) to the lysimeter measured PFOS porewater concentration. Overall these results highlight the potentially important role of air-water interfacial sorption on PFAS migration in AFFF-impacted unsaturated soils in an in situ field setting.

## Introduction

Poly- and perfluoroalkyl substance (PFAS) leaching to groundwater from unsaturated soils impacted with aqueous film forming foam (AFFF) is a recognized environmental issue at many former and current fire fighter training areas (Anderson et al., 2019; Anderson, 2021; Bräunig et al., 2019; Høisæter et al., 2019). Management of such sites is particularly challenging because PFAS porewater concentrations and mass flux to underlying groundwater are typically unknown. As recently described by Anderson (2021), approaches typically used for other classes of organic contaminants to estimate leaching and mass flux based on soil-water partitioning models may be inappropriate for PFASs. Sorption hysteresis (Chen et al., 2016; Zhi and Liu, 2018), kinetically-controlled sorption (Brusseau et al., 2019; Schaefer et al., 2021), and retention at air-water or oil-water interfaces (Lyu et al., 2018; Costanza et al., 2019; Schaefer et al., 2019) are among the reasons why commonly employed leaching estimation methods may fail for PFASs.

Several recent studies have focused on the issue of PFAS leaching from AFFF-impacted soils. Using drainage lysimeters (also termed field columns), and an agricultural soil spiked with perfluorooctanoic acid (PFOA) and perfluorooctane sulfonate (PFOS), Stahl et al. (2013) showed that 3.12% of the PFOA and 0.013% of the PFOS leached from the soil over a 5 year period. Examining historically contaminated soils (15 years since last AFFF application in a fire training area), Høisæter et al. (2019) measured PFOS vertical soil concentration profiles that demonstrated significant vertical PFOS attenuation, with estimated PFOS retardation factors through the unsaturated zone ranging from 16 to 42. Both of these studies demonstrate substantial retention of PFOS within the unsaturated zone source areas.

In contrast, McLachlan et al. (2019) showed much more rapid removal of PFOS via leaching through unsaturated soil, with 2% of PFOS removed from the soil within 72 days. Quinnan et al. (2021), examining AFFF-impacted unsaturated soils, performed saturated synthetic leaching precipitation testing on collected soil and compared results to PFOS concentrations measured in field-deployed lysimeters. For two paired locations, agreement between the leaching test and lysimeter-based porewater data was reasonable (within approximately 50%); for a third paired location, results differed by more than an order of magnitude.

Other recent studies further highlight potential complexities associated with PFAS leaching, and the associated challenges with both measuring and predicting PFAS leaching behavior. Borthakur et al. (2021) showed that freeze-thaw processes and natural soil colloids can accelerate PFAS leaching. Simulations performed by Zeng and Guo (2021) suggest that preferential flow can result in elimination of air-water interfaces and increase the rate of PFAS migration.

Collectively, these studies highlight the variability in PFAS leaching in unsaturated soils and the challenges in predicting PFAS leaching using currently available methods. Methods to predict and model PFAS porewater concentrations in AFFF source area leachates have yet to be demonstrated at the field scale. Furthermore, while much attention has been given to the potential role of the air-water interfacial accumulation on PFAS migration through unsaturated soils, field-scale data to confirm the importance of this mechanism is largely absent, thus models developed to describe the impacts of PFAS sorption at the air-water interface have yet to be validated *in situ* at historically contaminated sites. Because there is an immediate and pressing need to improve

109 understanding of PFAS leaching in AFFF-impacted source areas and to develop models
110 capable of predicting such leaching (Anderson et al., 2021), demonstrating and
111 quantifying the role of air-water interfacial sorption on PFAS migration at the field scale
112 is a high priority for advancing mechanistic understanding and supporting overall site
113 management. The objective of this study was to demonstrate a method for predicting
114 PFAS porewater concentrations in an AFFF-impacted source zone based on PFAS
115 migration models previously validated at the bench-scale (Lyu et al., 2018; Brusseau et
116 al., 2019b), and to demonstrate the role of air-water interfacial sorption on PFAS
117 porewater concentrations and ultimately PFAS mass flux to groundwater.
118
119 **Methods**
120 *Test Site*
121 An AFFF-impacted site in the northeastern United State that was used for foam
122 formulation testing (not actual firefighting with fuels) was selected for testing. The depth
123 to water at the site typically ranges from approximately 1.8 to 2.7 m below ground
124 surface (bgs). As previously described (Schaefer et al., 2021), unsaturated soil cores from
125 this site were collected for laboratory testing in January 2019, approximately 22 years
126 after the last known AFFF application; these soil cores were used to determine PFAS
127 concentration at the site, and to determine PFAS desorption isotherms. PFAS soil
128 properties are provided in Table S1. Soil PFAS concentrations have been previously
129 reported (Schaefer et al., 2021b) for the shallow homogenized interval from 0.03 to 0.9 m
130 below ground surface and for the deep homogenized interval from 0.9 to 2.4 m below
131 ground surface; these data are provided in Table S2.

Approximately 1.5 years after these soil cores were collected, a network of lysimeters were installed to facilitate in situ porewater collection. Lysimeters were installed in a 4.3 m x 4.3 m area of undisturbed soil (referred to as the test cell) that was hydraulically isolated using sheet-piling. Several ceramic porous cup suction lysimeters were installed, along with electrical resistance-based moisture probes, at various depths within the vadose zone with in. The test cell and lysimeters are shown in Figure S1. Figure 1 details the installed sampling equipment and instrumentation. Lysimeter depths are summarized in Table 1. A conceptual cross-section also is provided in Figure S2.

Porous cup suction lysimeters were purchased from Soil Moisture Equipment Corp. (Goleta, CA). The lysimeters used were constructed of PVC and had a diameter of 4.8 cm. The ceramic porous cup was 3.8 cm long with a 2 bar bubbling pressure; lysimeter lengths ranged from 0.3 m to1.5 m. Lysimeters were installed using hand augers. A silica flour (200 mesh) slurry was used in the lysimeter boreholes such that the annular space was filled with the silica flour several centimeters above the porous cup. A few centimeters of coarse sand was layered on top of the silica flour, and the remaining annular space was filled with medium-size bentonite chips to the ground surface. Lysimeters were connected to a vacuum manifold system for sample collection.

A bromide tracer was included with the silica flour slurry. After collecting an initial round of porewater samples to flush the system, the initial round of samples for PFAS analysis was collected. This initial round of samples for PFAS analysis also was analyzed for bromide. These measured bromide concentrations were less than 10% of initial bromide concentrations, indicating that the water captured in the lysimeters was representative of natural porewater that was not artificially diluted by the slurry water.

155 Parallel laboratory testing with both the lysimeters and silica fluor showed that PFOS
156 sorption to the silica flour and lysimeter was negligible.
157 Moisture probes (PR2/6 probes, manufactured by Delta-T Devices) were installed at 3
158 locations within the test cell. The moisture probes contained multiple sensors along the
159 vertical length of the probe that allowed for measurement of electrical potential at depths
160 of 20, 30, 60, and 100 cm. A rain gauge also was installed at the test site. A monitoring
161 well located in the center of the test cell was used to ensure that the water table remained
162 below the deepest installed lysimeters.
163
164 *Monitoring and Analyses*
165 Lysimeter sampling occurred using a vacuum manifold system, where a vacuum of
166 approximately 30 to 45 cb was applied over a set time interval of approximately 18 hours
167 to 5 days for each sampling event. As described in the installation details, purging of the
168 initial porewater collected within each lysimeter was performed to ensure that PFAS
169 concentrations measured in the collected samples were representative of porewater and
170 not moisture added during the lysimeter installation.
171 Three rounds of sampling were performed over a 49 day period (July 15, 2020 to
172 September 2, 2020), where the 11 lysimeters shown in Table 1 were sampled. Samples
173 were collected in 1 L glass bottles for each lysimeter within the manifold system.
174 Collected porewater volumes in each glass bottle typically ranged from 5 to 300 mL per
175 sampling event. Collected lysimeter porewater samples were transferred to 50 mL
176 polypropylene centrifuge tubes for PFAS analysis. Select samples were also analyzed for
177 total organic carbon (TOC) via combustion analysis, pH, and electrical conductivity.

178 PFAS analyses on the collected aqueous porewater samples was performed using an
179 Agilent 1260 series HPLC (Santa Clara, CA) and a SCIEX QTOF X500R (Framingham,
180 MA) using positive and negative mode electrospray ionization for analysis of
181 cationic/zwitterionic and anionic/zwitterionic compounds (respectively) via orthogonal
182 chromatography, as previously described in Barzen Hansen et al (2015). Additional
183 details of the PFAS analyses, including screening and semiquantitation of suspect
184 analytes, are described in the Supplemental Materials and Table S3.
185
186 *Bench-Scale Testing to Measure PFAS Sorption at the Air-Water Interface*
187 Laboratory bench-scale batch experiments were performed to determine values of
188 the air-water interfacial partition coefficient $K_{aw}$ (cm) for PFOS, PFHpS, and PFOA.
189 Values of $K_{aw}$ were directly measured using porewater collected from the lysimeters
190 using the film method, described in detail in Schaefer et al. (2019). Briefly, this method
191 entails filling a 25 cm diameter HDPE pan with approximately 2.2 L of the collected
192 porewater, allowing 3 days of equilibration, draining the bulk water (while collecting a
193 sample of this bulk water for PFAS analysis), and collecting the film of water remaining
194 in the pan (approximately 0.15 L) for PFAS analysis. PFOS, PFHpS, and PFOA
195 concentrations measured in the bulk porewater sample collected were 9,800, 310, and
196 400 ng/L, respectively. Applying a mass balance, and knowing the geometric surface area
197 of the air-water interface in the film residing in the pan, the PFAS mass per unit area at
198 the air water interface ($\beta$ in units of ng $cm^{-2}$) is determined. $K_{aw}$ is then calculated as $\beta$
199 divided by the bulk water concentration. This experiment was performed in duplicate.
200

## Results and Discussion

*Sample Collection and Porewater Characteristics*

The porewater saturations (S, in $cm^3$ per $cm^3$) and the three lysimeter temporal sampling intervals over which porewater was collected are shown in Figure 2; corresponding cumulative precipitation is shown in Figure S3. Porewater TOC, conductivity, and pH levels are summarized in Table S4. No significant correlation ($p>0.05$) between PFAS concentrations and the geochemical parameters in Table S4 was observed. Porewater samples were collected during a precipitation event, or within 3 days of a precipitation event. In all cases, evidence of water flux through the vadose zone was noted during sample collection by decreases in soil moisture as a function of time. It is unclear why a saturation reading of approximately 1.5 was measured at SMP-2(60 cm) during a severe storm event on August 11, 2020.

The water flux thorough the test cell was conservatively estimated for the well-drained sandy soils at the site by using the rainfall flux. As shown in Figure S3, 0.184 m of rainfall occurred over the 49 day monitoring period, resulting in an average water flux of $3.4 \times 10^{-3}$ m $d^{-1}$ through the test cell.

*PFAS Porewater Concentrations and Mass Flux*

Detected PFAS concentrations measured at each lysimeter for each of the 3 sampling events are presented in Table S5. Average PFAS concentrations over all 3 sampling events measured among the 5 lysimeters at a depth of 0.61 m bgs and also among the 4 lysimeters at a depth of 1.2 to 1.5 m bgs are shown in Figure 3. Lysimeters L-2 and L-8, installed at the very shallow depth below ground surface of 0.15 m, were not included in

224 Figure 3 because the shallow depth coupled with rapid water infiltration into the sandy
225 soil likely were not representative of equilibrium conditions and PFAS porewaters
226 impacting underlying groundwater; average PFAS concentrations in L-2 and L-8 over the
227 3 sampling events were approximately 4 standard deviations greater than the mean
228 calculated among the deeper lysimeters shown in Figure 3, suggesting these data were
229 outliers compared to the lysimeter data measured at depths of 0.61 m and 1.2 to 1.5 m
230 bgs. For example, the average PFOS concentration at 0.15 m over the 3 sampling events
231 was 45,000 ± 25,000 ng/L, which is more than 4 time greater than that measured in the
232 deeper lysimeters shown in Figure 3. In addition, lysimeter L-5 from the first round of
233 sampling was excluded because only a very limited volume of porewater (6.5 $cm^3$ of
234 porewater versus > 60 $cm^3$ for all other lysimeters) had been initially flushed through the
235 lysimeter prior to and including porewater collection associated with the first sampling
236 event, and PFAS concentrations were 5-times lower in L-5 than the average observed
237 among the other lysimeters. The subsequent round of sampling in L-5 yielded greater
238 than 200 $cm^3$ of porewater. Finally, for L-1, several PFAS results for the second and third
239 rounds of sampling (including results for PFOS, PFHpS, and PFOA) were excluded from
240 the averages shown in Figure 3 because measured PFAS concentrations were at least 3
241 standard deviations greater than then average calculated among the other lysimeters for
242 most of the PFASs detected. Overall, with these exceptions, results show that PFAS
243 concentrations measured in the porewater at depths of at least 0.61 m bgs were generally
244 repeatable among the lysimeters and over the 3 sampling events, as indicated by 95%
245 confidence intervals that were typically less than 50% of the average for the shallow

(0.61 m bgs) lysimeters, and less than 40% of the average for the deep (1.2 to 1.5 m bgs) lysimeters.

Results show that the PFAS concentrations measured in the shallow lysimeters located at 0.61 m bgs were typically statistically identical (overlapping 95% confidence intervals) to those measured at 1.2 to 1.5 m bgs, indicating that PFAS concentrations were at an apparent equilibrium in the percolating porewater within the interrogated depth interval of the vadose zone (i.e., PFAS concentrations in porewater not changing with depth). Thus, despite the comparatively higher organic carbon and PFAS concentrations associated with the shallow soil (Tables S1 and S2), PFAS concentrations in the porewater are in local equilibrium with the soil throughout the interrogated interval. This apparent local equilibrium suggests that independently determined equilibrium partitioning parameters may be useful for predicting PFAS porewater concentrations, as discussed in the following section.

PFOS and perfluorohexane sulfonate (PFHxS) were the PFASs that showed the highest average porewater concentrations in Figure 3 of approximately 10,000 and 25,000 ng $L^{-1}$, respectively, for the depths of 0.61 m and 1.2 – 1.5 m. PFOS and PFHxS were also the PFASs that had the highest concentrations in the soil (Table S2). The perfluoroalkyl acid (PFAA) mass flux through the test cell during the 49 day monitoring period is shown in Table 2. Extrapolated over the course of a year, the total mass of PFAAs leached from the unsaturated soil within a year would be 1.1 ± 0.37 g. Based on PFAA soil concentrations measured within the test cell (Table S2), this total annually leached PFAA mass represents only 2% of the total PFAS mass present in the unsaturated zone. These results suggest that PFAAs will persist in the unsaturated soils for decades to

269 come, although it is currently unclear how PFAA mass flux will diminish over time due
270 to thermodynamic and/or kinetic limitations.
271 Sporadic (<35% of lysimeter samples) detections of perfluorohexane sulfonamide
272 (FHxSA) were observed, but results were typically below the analytical method
273 quantification limit of 2,000 ng $L^{-1}$, which was much greater than the 200 ng $L^{-1}$ method
274 quantification limit for most PFAAs. When detected, FHxSA concentrations ranged from
275 5,000 to 10,000 ng $L^{-1}$. 6:2 Fluorotelomer sulfonate (6:2 FtS) was only sporadically
276 detected during the first 2 sampling events, but was measured at an average concentration
277 of approximately 2,000 ng $L^{-1}$ in the third round. It is currently unclear why these two
278 compounds were not detected on a more consistent level. No suspect PFAS analytes were
279 detected in the porewater, though this is likely due to the high degree of dilution required
280 for aqueous analysis due to the high PFHxS and PFOS levels.
281
282 *PFAS Mass Balance and Role of the Air-Water Interface*
283 Results of the film experiments yielded $K_{aw}$ values of 0.18 ± 0.029 cm, 0.071 ±
284 0.061 cm, 0.064 ± 0.048 cm for PFOS, PFHpS, and PFOA, respectively (average ± 95%
285 confidence intervals shown). The elevated $K_{aw}$ values for PFOS are expected due to its
286 increased perfluorinated chain length relative to PFHpS and PFOA (Schaefer et al.,
287 2019). $K_{aw}$ values for the other PFASs present in porewater were below that which could
288 be measured using the film method.
289 The ionic strength of the porewater solution, based on the average conductivity value
290 shown in Table S4, was 0.01 M. Figure 4 shows the measured PFOS porewater $K_{aw}$ value
291 compared to $K_{aw}$ values previously measured in electrolyte solutions (all using the

292 previously described film method). The PFOS $K_{aw}$ measured in the porewater (0.18 ±
293 0.029 cm) is identical to that measured in electrolyte in 0.01 M NaCl (0.18 ± 0.008 cm)
294 by Schaefer et al. (2019), suggesting that the porewater constituents (i.e., total organic
295 carbon, other PFASs) did not have a substantial impact on PFOS interfacial sorption for
296 the porewater examined in this study.
297 In response to a recent study that suggests the film method may overpredict $K_{aw}$
298 values for PFAS (Le et al., 2021), Figure 4 also shows results of a measured PFOS $K_{aw}$
299 value in a 0.003 M NaCl solution that was determined herein using the Garrett metal
300 screen method (Garrett, 1965; Daumas et al., 1976; Agogue′ et al. 2004); details of this
301 method are provided in the Supplemental Materials. The consistency between the Garrett
302 metal screen method and the film method data coupled with the associated model shown
303 in Figure 4 suggests that the film method is in fact appropriate for determining $K_{aw}$ values
304 for PFOS.
305 Figure 5 shows the average PFAS porewater concentrations (average of values shown
306 in Figure 3) lysimeters compared to predicted values of the PFAS porewater
307 concentrations. Only PFASs that were both consistently detected in the lysimeters
308 samples (Figure 3), and also shown to be at equilibrium in the batch kinetic desorption
309 testing (Schaefer et al., 2021), were evaluated. Predicted PFAS porewater concentrations
310 are based conceptually on the PFAS mass balance model developed by Brusseau et al.
311 (2019b), which considers PFAS distribution among the soil, aqueous phase, and air-water
312 interface. The application of the model is based on two key parameters: a desorption $K_d$
313 value to describe PFAS soil-water partitioning and a PFAS interfacial partition
314 coefficient ($K_{aw}$) to describe PFAS partitioning to the air-water interface. The following 3

equations were used to describe PFAS phase behavior among the soil, aqueous, and air-water interfacial phases in a 10 g unit mass of shallow soil (50% saturation based on moisture probe and soil moisture data):

$$K_{aw} = \frac{\beta}{C} \quad \text{Eq. 1}$$

$$K_d = \frac{C_s - b}{C} \quad \text{Eq. 2}$$

$$M_T = Mass\ at\ interface + Mass\ in\ soil = V\beta a_{aw} + C_s m \quad \text{Eq. 3}$$

where C is the aqueous concentration (ng $cm^{-3}$), $C_s$ is the sorbed soil concentration (ng $kg^{-1}$), $M_T$ is the total PFAS mass used in a 10 x $10^{-3}$ kg mass of soil (ng, determined on a dry soil basis by multiplying the total PFAS concentrations in the collected soil shown in Table S2 by the 10 x $10^{-3}$ kg of dry soil), V is the *in situ* soil bed volume associated with the 10 x $10^{-3}$ kg of dry soil (6.1 $cm^3$, estimated assuming a dry bulk density of 1.65 g $cm^{-3}$), $a_{aw}$ is the air water interfacial area per bed volume ($cm^2$ per $cm^3$), and m is the mass of dry soil (10 x $10^{-3}$ kg). Desorption isotherms using the shallow soil described herein were previously determined using a sequential batch dilution technique to determine $K_d$ (PFAS soil sorption coefficient in L $kg^{-1}$) and b (the y-intercept associated with the linear desorption isotherm in L $kg^{-1}$ (Schaefer et al., 2021b); these values are provided in Table 3. It is noted that Eq. 3 neglects the mass contribution from the aqueous phase. Based on the measured soil concentration and PFAS porewater concentrations, the PFAS mass in the water accounts for less than 1% of the total mass, thus justifying this simplification. Based on the amount of rainfall between soil collection and the time lysimeter sampling was initiated (approximately 142 cm of rainfall over 18 months based on weather station data), and using the leachate concentrations in Figure 3, the mass of PFOS and PFHpS

leached from the soil between the time of soil collection and the beginning of the lysimeter sample collection 18 months later is estimated at less than 1% and 2% of their mass present in the saturated zone, respectively. Thus, this small amount of mass removal was considered negligible for the model. For PFOA, using this same approach, the mass removal over this 18 month period is estimated at 15%. To account for this, $M_T$ for PFOA in Eqs. 2 and 3 was decreased by 15% to provide a more appropriate value for the model.

The value for $a_{aw}$ was determined based on the average soil grain size using the following equation (Lyu et al., 2018; Brusseau et al., 2019):

$$a_{aw} = 3.9d^{-1.2}(1 - S) \quad \text{Eq. 4}$$

where d is the mean particle diameter of the shallow soil (0.04 cm) and S is the pore saturation of the soil during lysimeter sample collection (estimated at 0.5 $cm^3$ $cm^{-3}$ based on moisture probe data). The resulting value for $a_{aw}$ is 93 $cm^{-1}$. A discussion of the error associated with the model predictions is provided in the Supplemental Materials.

As depicted in Figure 5, if PFAS sorption to the air-water interface is not considered, the predicted PFAS porewater concentrations are 1.4- to 4-times greater than the PFAS concentrations measured in porewater. PFOS shows the greatest discrepancy in aqueous concentration between the lysimeter-based and batch desorption-based results among the PFASs examined. PFOS is the most surface active among the three PFASs shown in Figure 5 (Costanza et al., 2019; Schaefer et al., 2019). These observations suggest the possibility that the discrepancy between lysimeter and batch desorption results is due to PFAS accumulation at air-water interfaces, which are present in the unsaturated soils within the test cell.

361 Figure 5 also shows that including PFAS retention at the air-water interface results in
362 a substantial improvement in the prediction of PFAS porewater concentrations, most
363 notably for PFOS where a 58% reduction in the predicted porewater concentration was
364 observed. When considering uptake at the air-water interface, the predicted porewater
365 PFOS concentration is within the 95% confidence interval of the measured PFOS
366 porewater concentration. PFOS showed a much greater measured interfacial partition
367 coefficient ($K_{aw}$=0.18 cm) than PFHpS (0.071 cm) and PFOA (0.064 cm) in porewater,
368 thus inclusion of air-water interfacial sorption expectedly had the most notable effect on
369 PFOS.
370 For PFHpS, inclusion of air-water interfacial sorption also resulted in a predicted
371 value that was within the 95% confidence interval of the measured porewater value,
372 whereas exclusion of air-water interfacial sorption resulted in a significant overprediction
373 of the measure porewater value. For PFOA, the relatively large uncertainty associated
374 with the soil-water partitioning ($K_d$ value) limited the ability to conclusively assess any
375 improvement in porewater prediction by including sorption at the air-water interface.
376 Together, these measured values and calculations provide a line of evidence for the
377 relevance of PFAS air-water interfacial sorption *in situ*. To our knowledge, these are the
378 first field data that demonstrate the impact of PFAS air-water interfacial sorption on
379 PFAS leaching, thereby validating bench-scale studies that suggest air-water interfacial
380 sorption is an important mechanism to consider at AFFF-impacted sites.
381 While, particularly for PFOS and PFHpS, inclusion of the air-water interfacial
382 sorption resulted in improved predictions of *in situ* porewater concentration, it is possible
383 that factors besides sorption at the air-water interface could have played a role in the

384 overpredictions shown in Figure 5. These factors include flow heterogeneity and other
385 mass transfer limitations. However, given the similarity in PFAS concentrations between
386 the shallow and deep lysimeters (which suggests mass transfer effects were limited), as
387 well as the fact that the most surface active compound examined (PFOS) showed the
388 greatest improvement when the model included interfacial sorption, it is likely that air-
389 water interfacial sorption was the primary factor responsible for the discrepancy between
390 the measured porewater values and the $K_d$-only partitioning model shown in Figure 5.
391 Additional studies at a variety of sites are needed to further validate the role of interfacial
392 sorption on PFAS concentrations in porewater.
393
394 *Environmental Implications*
395 Results presented herein show that PFAS mass flux to underlying groundwater is
396 likely being reduced by 1.5- to 4-times for PFOS, PFHxS, and PFOA due to
397 accumulation at the air water interface, as highlighted by the impact of air-water retention
398 on PFAS porewater concentrations. Thus, consistent with previously performed
399 unsaturated column experiments (e.g., Lyu et al., 2018), air-water interfacial uptake plays
400 an important role in PFAS transport through the unsaturated zone. While the overall
401 PFAS mass flux from the AFFF-impacted soils remains largely controlled by desorption
402 from the soil, accounting for PFAS accumulation at the air-water interface is required to
403 estimate overall PFAS mass flux. Further study is needed to more closely examine the
404 impacts of variable saturation and water flux on PFAS mass flux through the vadose
405 zone. Further study also is needed to assess PFAS mass flux under differing soil,
406 hydraulic, and PFAS loading conditions.

**Acknowledgments**

Support for this research was provided by the Strategic Environmental Research and Development Program (SERDP) under Projects ER18-1204 and ER19-1205. Views, opinions, and/or findings contained in this report are those of the authors and should not be construed as an official Department of Defense position or decision unless so designated by other official documentation.

Supplemental Materials include a description of the PFAS analyses, information on additional testing to confirm the film method for determining $K_{aw}$, a description of the uncertainty for the model parameters, Tables S1 through S5, and Figures S1 through S2.

**References**

Anderson, R.H. The Case for Direct Measures of Soil-to-Groundwater Contaminant Mass Discharge at AFFF-Impacted Sites. *Environ. Sci. Technol*. **2021**, 55, 6580-6583.

Anderson, R. H., Adamson, D.T., Stroo, H.F. Partitioning of poly- and perfluoroalkyl substances from soil to groundwater within aqueous film-forming foam source zones. *J. Contam. Hydrol*. **2019**, 220, 59–65.

Barzen-Hanson, K. A.; Field, J.A. (2015). Discovery and implications of C2 and C3 perfluoroalkyl sulfonates in aqueous film-forming foams and groundwater. *Environ. Sci. Technol. Letters* **2015**, 2, 95-99.

Borthakur, A., Olsen, P., Dooley, G., Cranmer, B.K., Rao, U., Hoek, E.M., Blotevogel, J., Mahendra, S. and Mohanty, S.K. Dry-wet and freeze-thaw cycles enhance PFOA leaching from subsurface soils. *J. Haz. Mater. Letters* **2021,** 100029.

Bräunig, J., Baduel, C., Barnes, C.M. and Mueller, J.F. Leaching and bioavailability of selected perfluoroalkyl acids (PFAAs) from soil contaminated by firefighting activities. *Sci. Total Environ.* **2019**, 646, 471-479.

Brusseau, M.L., Khan, N., Wang, Y., Yan, N., Van Glubt, S. Carroll, K.C. Nonideal transport and extended elution tailing of PFOS in soil. *Environ. Sci. Technol***. 2019**, 53, 10654-10664.

Brusseau, M.L., Yan, N., Van Glubt, S., Wang, Y., Chen, W., Lyu, Y., Dungan, B., Carroll, K.C., Holguin, F.O. Comprehensive retention model for PFAS transport in subsurface systems. *Water Res.* **2019b**, 148, 41-50.

Chen, H., Reinhard, M., Nguyen, V.T., Gin, K.Y.H. Reversible and irreversible sorption of perfluorinated compounds (PFCs) by sediments of an urban reservoir. *Chemosphere* **2016**, 144, 1747-1753.

Costanza, J., Arshadi, M., Abriola, L.M. Pennell, K.D. Accumulation of PFOA and PFOS at the air–water interface. *Environ. Sci. Technol Lett.* **2019**, 6, 487-491.

Daumas, R. A., P. L. Laborde, J. C. Marty, and A. Saliot. Influence of sampling method on the chemical composition of water surface film. *Limnol. Oceanogr.* **1976**, 2, 319-326.

Garrett, W. D. Collection of slick-forming materials from the sea surface. *Limnol. Oceanogr*. **1965**, 10, 602-605.

Høisæter, Å., Pfaff, A. and Breedveld, G.D. Leaching and transport of PFAS from aqueous film-forming foam (AFFF) in the unsaturated soil at a firefighting training facility under cold climatic conditions. J. Contam. Hydrol. **2019**. 222, 112-122.

Le, S.T., Gao, Y., Kibbey, T.C., Glamore, W.C. and O'Carroll, D.M.. A new framework for modeling the effect of salt on interfacial adsorption of PFAS in environmental systems. *Sci. Total Environ.* **2021**, 796, 148893.

Lyu, Y., Brusseau, M.L., Chen, W., Yan, N., Fu, X. Lin, X. Adsorption of PFOA at the air–water interface during transport in unsaturated porous media. *Environ. Sci. Technol*. **2018**, 52, 7745-7753.

McLachlan, M.S., Felizeter, S., Klein, M., Kotthoff, M. De Voogt, P. Fate of a perfluoroalkyl acid mixture in an agricultural soil studied in lysimeters. *Chemosphere* **2019**, 223, 180-187.

Quinnan, J., Rossi, M., Curry, P., Lupo, M., Miller, M., Korb, H., Orth, C., Hasbrouck, K. Application of PFAS-mobile lab to support adaptive characterization and flux-based conceptual site models at AFFF releases. *Remediation J*. 2021, 1-20.

Schaefer, C.E., Culina, V., Nguyen, D. Field, J. Uptake of Poly-and Perfluoroalkyl Substances at the Air–Water Interface. *Environ. Sci. Technol*. **2019**, 53, 12442-12448.

Schaefer, C.E., Nguyen, D., Christie, E., Shea, S., Higgins, C.P. Field, J.A. Desorption of Poly-and Perfluoroalkyl Substances from Soil Historically Impacted with Aqueous Film-Forming Foam. *J. Environ. Engin.* **2021**, 147, 06020006.

Schaefer, C.E., Nguyen, D., Christie, E., Shea, S., Higgins, C.P. Field, J.A. Desorption Isotherms for Poly- and Perfluoroalkyl Substances in Soil Collected from an Aqueous Film- Forming Foam Source Area. Forthcoming *J. Environ. Engin.* **2021b** DOI: 10.1061/(ASCE)EE.1943-7870.0001952

Stahl, T., Riebe, R.A., Falk, S., Failing, K., Brunn, H. Long-term lysimeter experiment to investigate the leaching of perfluoroalkyl substances (PFASs) and the

carry-over from soil to plants: results of a pilot study. *J. Agri. Food Chem.* **2013**, 61, 1784-1793.

Zeng, J. and Guo, B. Multidimensional simulation of PFAS transport and leaching in the vadose zone: Impact of surfactant-induced flow and subsurface heterogeneities. *Advan. Wat. Resour.* **2021**, 155, 104015.

Zhi, Y.; Liu, J. X., Sorption and desorption of anionic, cationic and zwitterionic polyfluoroalkyl substances by soil organic matter and pyrogenic carbonaceous materials. *Chem. Engin. J.* **2018,** 346, 682-691.

# TABLES

**Table 1.** Lysimeter depths. Lysimeters L-2 and L-8, installed at the very shallow depth below ground surface of 0.15 m, also were not used in this study. This shallow depth, coupled with rapid water infiltration into the sandy soil, likely were not representative of equilibrium conditions and PFAS porewaters impacting underlying groundwater. All lysimeters were placed within either the shallow (0.03 to 0.9 m) or deep (0.9 to 2.4 m) soil intervals, as described in Table S2.

| **Lysimeter** | **Depth (m below ground surface)** |
|---|---|
| L-1 | 0.61 |
| L-2 | 0.15 |
| L-3 | 0.61 |
| L-4 | 1.5 |
| L-5 | 0.61 |
| L-6 | 1.5 |
| L-7 | 1.2 |
| L-8 | 0.15 |
| L-9 | 0.61 |
| L-10 | 1.2 |
| L-11 | 0.61 |

**Table 2.** Calculated PFAS mass flux through the vadose zone towards underlying groundwater based on an average water flux of 3.4 x $10^{-3}$ m $d^{-1}$ and the average PFAS concentrations for the deep lysimeters at 1.2 to 1.5 m bgs.

| **PFAS** | **Mass Flux (ng $m^{-2}$ $d^{-1}$)** |
|---|---|
| PFBS | 6,400 ± 1,800 |
| PFPeS | 13,000 ± 2,900 |
| PFHxS | 92,000 ± 32,000 |
| PFHpS | 750 ± 360 |
| PFOS | 28,000 ± 11,000 |
| PFBA | 1,400 ± 470 |
| PFPeA | 3,500 ± 860 |
| PFHxA | 12,000 ± 3,300 |
| PFHpA | 3,100 ± 980 |
| PFOA | 1,800 ± 805 |

**Table 3.** Regressed values of $K_d$ and y-intercept (b) with 95% confidence intervals for shallow soil in the interval of 0.03 to 0.9 m below ground surface, as determined by Schaefer et al. (2021b).

| PFAS | $K_d$ ($L\ kg^{-1}$) | b ($ng\ kg^{-1}$) |
|---|---|---|
| PFOA | 2.2 ± 1.1 | 3,000± 1,100 |
| PFHpS | 3.2 ± 1.2 | 17,000± 6,000 |
| PFOS | 6.9 ± 1.5 | 1,000,000 ± 330,000 |

# FIGURES

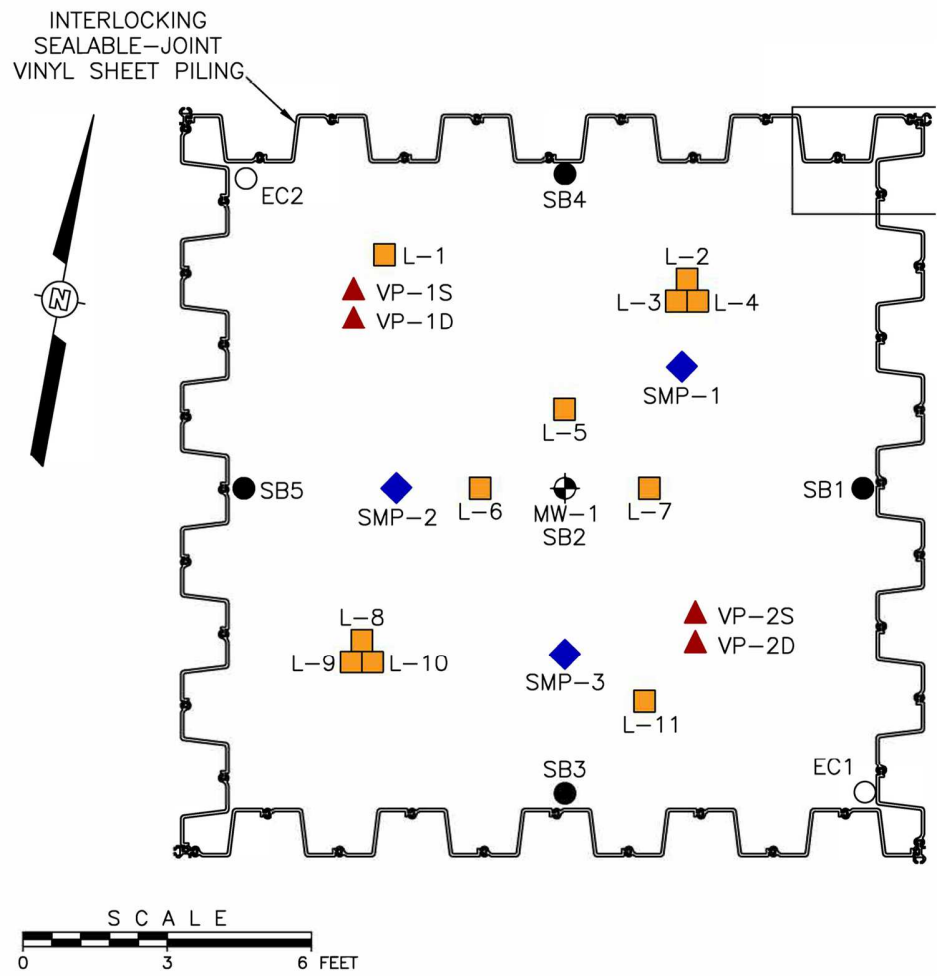


**Figure 1**. Details of installed system components. L-1 through L-11 are the lysimeters. SMP-1 though SMP-3 are the soil moisture probe locations. VP indicates locations for vapor probes. EC1 and EC2 indicate locations where electrical conductivity probes were used, and SB1 through SB5 are soil bore locations. MW-1 is a shallow monitoring well used to monitor the water table elevation.

559 a.

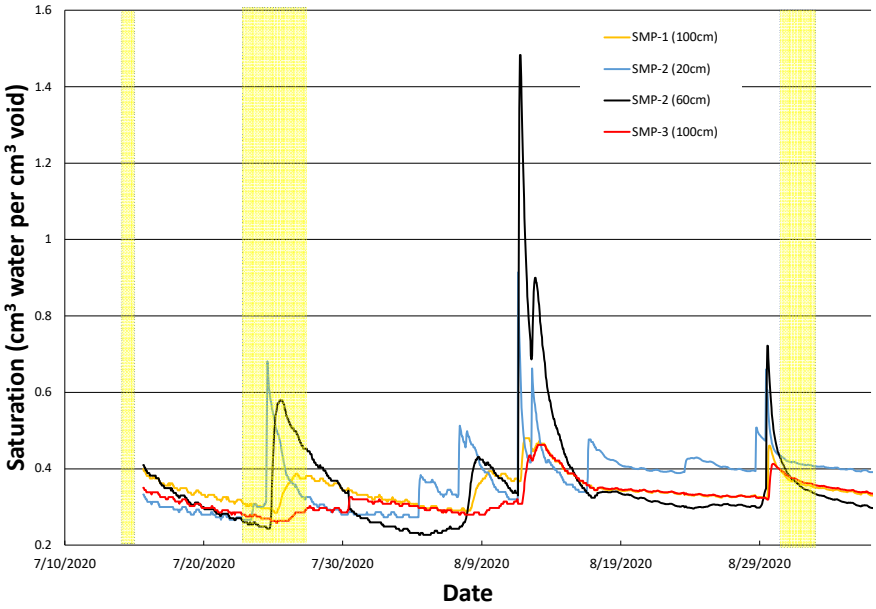


560

561 b.

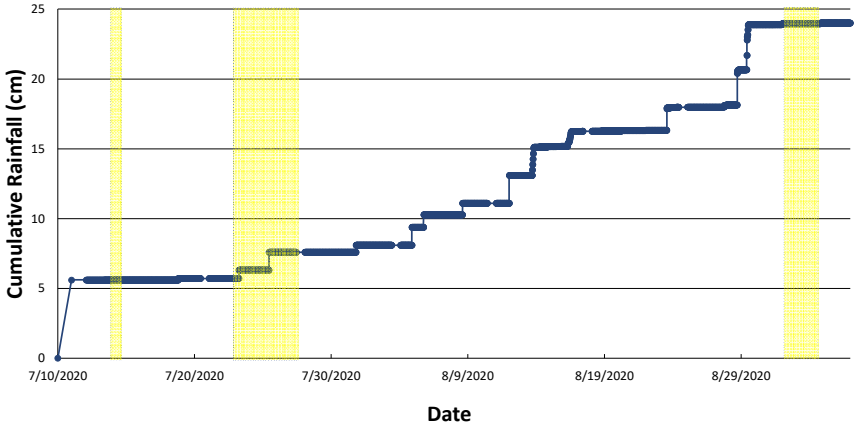


562

563 **Figure 2**. **a.** Lysimeter sampling intervals and corresponding water saturations (measured
564 using the moisture probes) over the study period. The three shaded bars indicate the
565 sampling intervals over which lysimeter samples were collected via an applied vacuum.
566 Lysimeter samples were collected during or shortly after rainfall events where the soil
567 moisture and vertical water flow remained elevated. Saturation values were calculated
568 based on calibration to soil moisture contents obtained via direct collection of soil
569 samples.
570 **b**. Lysimeter sampling intervals and cumulative precipitation over the study period. The
571 installed rain gauge was only operational after 8/16/20; a local weather station (data
572 provided at https://www.cocorahs.org/) was used to monitor rainfall prior to this date.

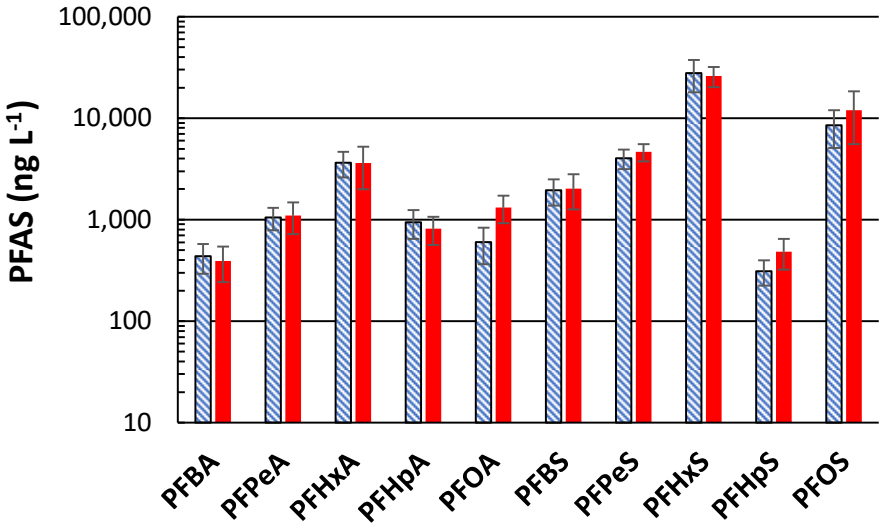


**Figure 3.** Average PFAS porewater concentrations measured using the field-deployed lysimeters over three rounds of sampling. The blue-hatched bars are from the 4 deep (1.2 to 1.5 m bgs) lysimeters, and the red bars are from 4 shallow (0.61 m bgs) lysimeters. As described in the text, the first round of sampling from L-5 and outliers (> 3 standard deviations from the mean) from the second and third rounds of sampling at L-1 were excluded from calculation of the averages shown in this figure. Error bars represent 95% confidence intervals. PFBA =perfluorobutanoic acid, PFPeA = perfluoropentanoic acid, PFHxA = perfluorohexanoic acid, PFHpA =perfluoroheptanoic acid, PFOA = perfluorooctanoic acid, PFBS =perfluorobutanesulfonate, PFPeS=perfluoropentanesulfonate, PFHxS = perfluorohexanesulfonate, PFHpS= perfluoroheptanesulfonate, and PFOS = perfluorooctanesulfonate.

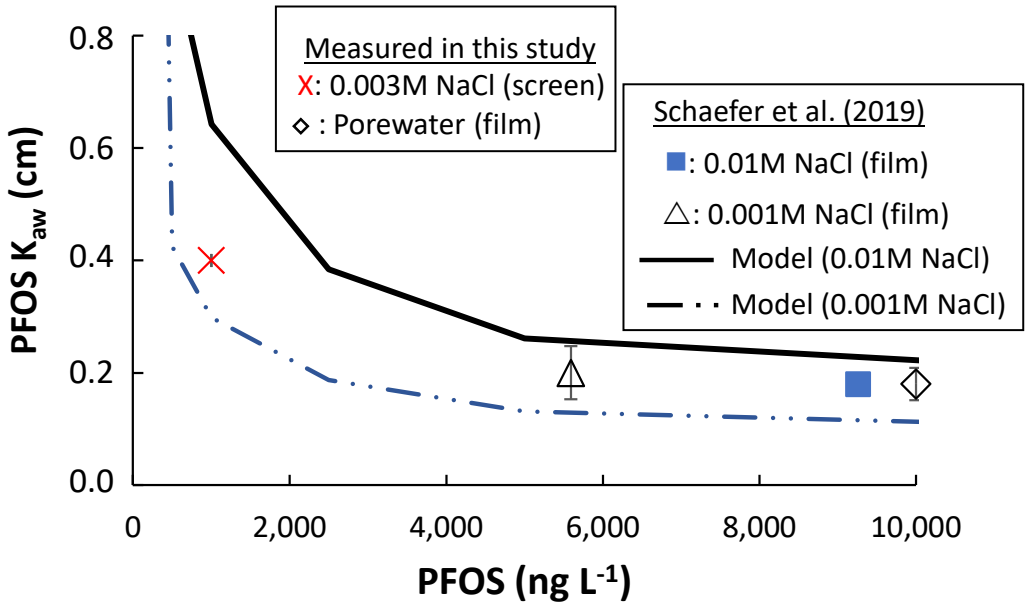


**Figure 4**. $K_{aw}$ for PFOS in porewater (0.01 M ionic strength) compared to PFOS $K_{aw}$ values previously measured in similar ionic strength electrolyte solutions using the film method. The PFOS $K_{aw}$ in 0.003 M NaCl measured herein using the Garrett metal screen method also is shown for comparison. All measured $K_{aw}$ values reside within the Freundlich-based model predictions at 0.01M and 0.001 M determined by Schaefer et al. (2019). Error bars represent 95% confidence intervals. In some cases, the error bars are smaller than the symbol.

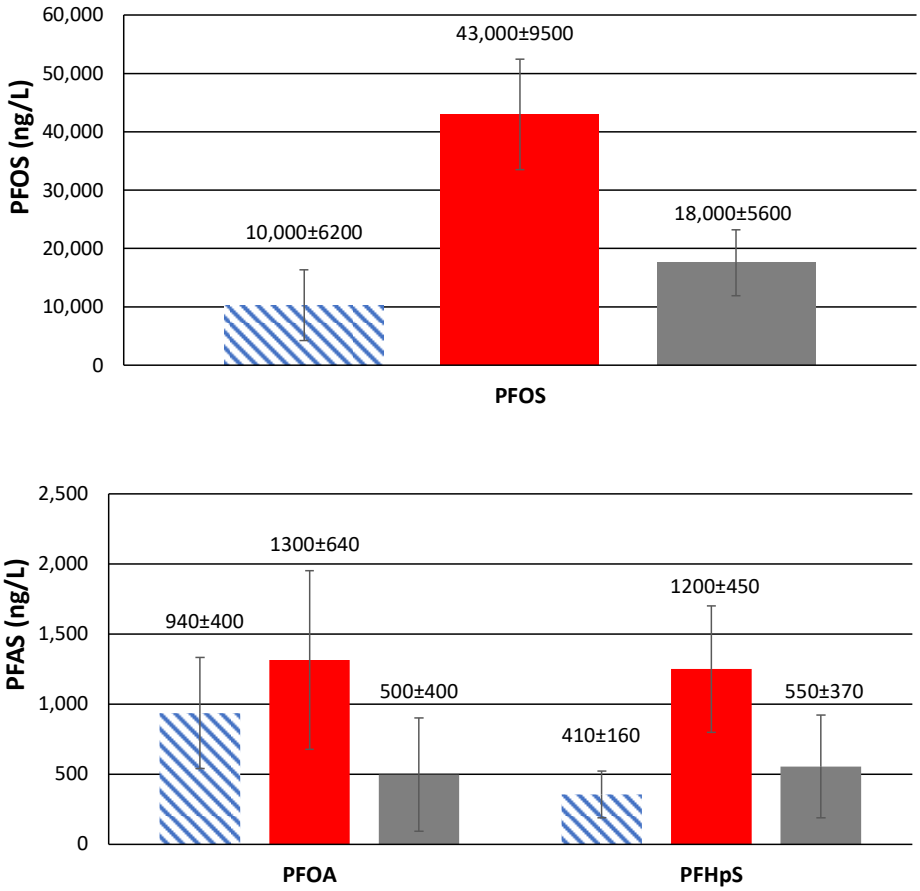


601

602 **Figure 5**. PFAS average porewater concentrations for PFOS, PFHpS, and PFOA over all
603 three rounds of sampling (blue hatched bars) using the measured lysimeter data shown in
604 Figure 3. Results are compared to predicted porewater PFAS concentrations that exclude
605 (red bars) or include (gray bars) PFAS sorption to the air-water interface. Error bars for
606 the measured porewater concentrations represent 95% confidence intervals using the
607 shallow (0.61 m bgs) lysimeters over all three sampling rounds. Error bars for the
608 predicted values represent 95% confidence intervals, which are calculated based on
609 propagation of the error (95% confidence intervals) associated with the measured $K_d$ and
610 $K_{aw}$ values, and the estimated $a_{aw}$ value, as described in the Supplemental Materials.
611 Values shown above bars are the aqueous concentration ± 95% confidence intervals.

**Abstract Art**